SET Domain Bifurcated Histone Lysine Methyltransferase 1 Regulates Histone Modification and DNA Damage Response during Zygotic Genome Activation in Pigs

Hyeon-Ji Song [1#], Song-Hee Lee [1#], Cheng-Lin Zhan [1], Qin-Yue Lu [1], Gyu-Hyun Lee [1], Jae-Min Sim [1], Yu-Jin Jo [2], Ji-Su Kim [2] and Xiang-Shun Cui [1,*]

[1] *Department of Animal Science, Chungbuk National University, Cheongju, Chungbuk, 28644, Republic of Korea*

[2] *Primate Resources Center (PRC), Korea Research Institute of Bioscience and Biotechnology (KRIBB), Nengme-gil 351-33, Jeongeup-si, Jeollabuk-do, 56216, Republic of Korea*

# These authors contributed equally to this work.

*** Corresponding author:** Xiang-Shun Cui (xscui@cbnu.ac.kr), Tel: +82 43-261-3751

uncorrected proof

Abstract

SET domain bifurcated histone lysine methyltransferase 1 (SETDB1) is a key epigenetic regulator that catalyzes histone H3 lysine 9 trimethylation (H3K9me3), a mark essential for transcriptional repression and heterochromatin formation. Here, we investigated the role of SETDB1 during zygotic genome activation (ZGA) in porcine embryos. SETDB1 knockdown (KD) was induced by microinjecting double-stranded RNA (dsRNA), and its impact on early embryonic development was evaluated. SETDB1 KD decreased H3K9me3 levels, markedly increased H3K9ac, and downregulated ZGA-associated genes. These epigenetic alterations were accompanied by impaired cleavage, reduced blastocyst formation, and a lower total cell number. Upon etoposide-induced DNA double-strand breaks, SETDB1 KD embryos showed reduced expression of key DNA repair proteins, failed to efficiently restore DNA integrity, and exhibited increased apoptosis, indicating a compromised DNA damage response and repair process. SETDB1 KD also reduced HDAC3 expression, suggesting that SETDB1 may regulate HDAC3 to maintain histone acetylation balance. Consistently, HDAC3 inhibition increased H3K9ac, decreased H3K9me3, and reduced SETDB1 protein levels, supporting a reciprocal regulatory relationship. Together, these findings indicate that SETDB1 is important for porcine embryonic development by coordinating histone modifications and safeguarding genomic integrity during ZGA, and they suggest that the interplay between SETDB1 and HDAC3 constitutes a potentially important epigenetic axis for proper histone modification dynamics and developmental competence.

Keywords: SETDB1, Histone modification, Zygotic genome activation, DNA damage repair, porcine embryos, HDAC3

Uncorrected proof

1. Introduction

Epigenetics regulates gene expression without altering the DNA sequence and plays critical roles in development, aging, and disease (Gibney and Nolan, 2010). Major epigenetic mechanisms include DNA methylation, non-coding RNAs, and histone modifications. Among these, dynamic changes in histone marks are particularly important during early embryogenesis to ensure proper zygotic genome activation (ZGA) (Bure et al., 2022).

Among the major epigenetic mechanisms, histone modifications represent a central regulatory process that modulates chromatin dynamics during early embryonic development. These modifications primarily occur at the N-terminal tails of histones, which contain amino acid residues such as lysine and arginine. These modifications are catalyzed by specific enzymes and influence chromatin structure, thereby regulating the accessibility of transcription factors and co-factors to DNA (Gelato and Fischle, 2008; Sinha et al., 2023; Zhang et al., 2015). Histone H3 lysine 9 trimethylation (H3K9me3) plays a well-known role in transcriptional silencing and heterochromatin formation. SET domain bifurcated histone lysine methyltransferase 1 (SETDB1) is one of the primary enzymes responsible for catalyzing H3K9me3. In somatic cells, SETDB1 has been implicated in maintaining transcriptional

uncorrected proof

repression, retrotransposon silencing, and X-chromosome inactivation (Prashanth et al., 2024). Previous studies showed that SETDB1 and HDAC3 act sequentially to regulate the histone modification mark H3K9me3 (Price et al., 2020). Once HDAC3 deacetylates H3K9, SETDB1 subsequently catalyzes its trimethylation. Thus, HDAC3 and SETDB1 function in a coordinated manner to establish the H3K9me3-mediated chromatin state.

Previous studies have shown that another H3K9-specific methyltransferase, Suppressor of Variegation 3-9 Homolog 1 (SUV39H1), facilitates the recruitment of heterochromatin protein 1 beta (HP1β) and DNA repair factors such as Tat-interactive protein 60 (TIP60) and Ataxia Telangiectasia Mutated (ATM) kinase to sites of double-strand breaks (DSBs) through the deposition of H3K9me3 (Liu et al., 2013). This evidence supports a model in which repressive histone modifications are involved not only in transcriptional silencing but also in chromatin-based signaling required for DNA damage response (DDR). During the maternal-to-zygotic transition, embryos undergo ZGA, a critical period marked by extensive chromatin remodeling and heightened vulnerability to DNA damage (Musson et al., 2022; Schulz and Harrison, 2019; Wyatt et al., 2022). Proper DDR during this stage is essential to preserve genome integrity and ensure normal embryonic development.

In mice, SETDB1 has been shown to participate in DDR and meiotic sex chromosome silencing, thereby acting as a molecular bridge between DNA repair and transcriptional

Uncorrected proof

repression in a sex-specific context (Hirota et al., 2018; Kim et al., 2016). These findings suggest that SETDB1-mediated heterochromatin regulation may be conserved across mammalian species. However, whether such functions extend to the ZGA stage during early embryogenesis remains poorly understood. In this study, we aimed to investigate the functional role of SETDB1 during ZGA in porcine embryos. By analyzing changes in histone modification and DNA damage repair-related proteins after SETDB1 KD, we sought to determine whether SETDB1 contributes to chromatin regulation and genome stability during this critical developmental period (Song., 2025).

uncorrected proof

2. Materials and Methods

2.1 Ethics statement

All animal procedures were conducted in compliance with the ethical guidelines and approved by the Institutional Animal Care and Use Committee (IACUC) at Chungbuk National University, Republic of Korea. In this study, only post-mortem porcine ovarian tissues obtained from a local abattoir were used, and no live animals were involved.

2.2 Antibodies

Rabbit anti-SETDB1 (Cat# 11231-1-AP; for Western blot) was purchased from Proteintech. Rabbit anti-Histone H3 (acetyl K9) (Cat# ab32129) and mouse anti-Histone H3 (tri methyl K9) (Cat# ab184677) were purchased from Abcam. Rabbit anti-HP1 beta (Cat# A22708), rabbit anti-Tip60 (Cat# A1678), rabbit anti-Phospho-ATM (S1918) (Cat# AP0008), and rabbit anti-HDAC3 (Cat# A19537) were purchased from Abclonal. Rabbit anti-Phospho-Histone H2A.X (Ser139) (Cat# 2577S) and rabbit anti-GAPDH (Cat# 5174S) were purchased from Cell Signaling Technology. Mouse anti-SETDB1 (Cat# sc-166621; used for immunofluorescence staining) was purchased from Santa Cruz Biotechnology. Alexa Fluor 488™ donkey anti-

uncorrected proof

mouse IgG (H + L) and Alexa Fluor 546™ donkey anti-rabbit IgG (H + L) were purchased from Invitrogen.

2.3 Drug treatments

To inhibit HDAC3, RGFP966 (CAS# 1357389-11-7, MedChemExpress, NJ, USA) was applied at final concentrations of 0 μM (control), 0.5 μM, and 1.0 μM. A preliminary test using 0 μM, 1 μM, 10 μM, and 100 μM (three replicates each) showed average developmental rates of 38.05%, 20.15%, 0.02%, and 0%, respectively. Based on the literature and our preliminary experiments (Ma et al., 2024; Wang et al., 2024), 0.5 μM and 1.0 μM were selected, together with the control, for the main experiments to assess dose-dependent effects. To induce DSBs in embryos, etoposide (ETP) (Cas# 33419-42-0, Sigma-Aldrich, St. Louis, USA) was applied at a concentration of 25 μg/mL, following a previous study (Wang et al., 2015). Parthenogenetic embryos were cultured in IVC medium containing 25 μg/mL etoposide for 5 h immediately after cytochalasin B removal, followed by washing and further culture in fresh IVC medium.

2.4 Oocyte Collection and in vitro maturation (IVM)

Uncorrected proof

Porcine ovaries from a local abattoir (Farm Story Dodram B&F, Chungbuk, South Korea) were transported in saline with antibiotics at 38°C. Cumulus-oocyte complexes (COCs) were aspirated from 3–6 mm follicles. ~50 COCs were matured in TCM-199 with 10% PFF, hCG, PMSG, sodium pyruvate, and cysteine [TCM-199 (11150-059, Gibco, NY, USA) supplemented with 10 ng/mL epidermal growth factor, 0.1 g/L sodium pyruvate, 10 IU/mL luteinizing hormone (LH), 0.57 mM L-cysteine, 10 IU/mL follicle-stimulating hormone, and 10% (v/v) porcine follicular fluid] at 38.5°C and 5% CO_2 for 44 h.

2.5 Parthenogenetic activation and in vitro culture (IVC)

Following IVM, cumulus cells were placed in 1 mg/mL hyaluronidase and pipetted about 50 times to remove cumulus cells. cumulus cells were removed with 1 mg/mL hyaluronidase. Oocytes with a visible first polar body were washed (DPBS + 0.1% BSA) and activated in a mannitol-based medium. Electrical activation was applied (110 V/cm, 60 μs × 2) using a BTX ECM 2001. Activated oocytes were cultured for 3 h in PZM-5 with 7.5 μg/mL cytochalasin B to prevent extrusion of the pseudo-second polar body. After washing, embryos were cultured in PZM-5 + 4 mg/mL BSA at 38.5°C, 5% CO_2, and development to the blastocyst stage was monitored at the 2-cell (Day 1), 4-cell (Day 2), and blastocyst (Day 7) stages. On Day 7,

uncorrected proof

embryos exhibiting a clearly defined blastocoel cavity were classified as blastocyst and collected for analysis, consistent with established criteria (Cockburn and Rossant, 2010).

2.6 Real-time reverse transcription–polymerase chain reaction

Total RNA was isolated from pooled embryos, with approximately 50 embryos used for each group, using the Dynabeads mRNA Direct Kit (Thermo Fisher Scientific, Waltham, USA). cDNA was synthesized using the ReverTra Ace kit (TOYOBO, Osaka, Japan). qPCR was performed on a CFX96 Real-Time PCR system (Bio-Rad) using the WizPure™ qPCR Master Kit (SYBR Green, Wizbiosolutions, Cheonju, Korea). Each reaction contained 10 μL 2× SYBR mix, 0.4 μL of each primer (10 μM), 1 μL cDNA, and 8.2 μL water. Cycling conditions were 95°C for 3 min, followed by 40 cycles of 95°C for 10 s and 60°C for 30 s (Kim et al., 2024). Relative expression was calculated using the 2^−ΔΔCt method with GAPDH as reference. The primers are as follows. *SETDB1* (F: CACACGCCAGTTCTACGATG, R: CCCAGCTCGAATTCTCTTGC), *ZSCAN4* (F: CTTGTTTGGTCCTCGAACAGT, R: TTCATGCCATCGTCTGTCAGGT), *TCSTV3* (F: AGAAAGGGCTGGAACTTGTGACCT, R: AAAGCTCTTTGAAGCCATGCCCAG), *RIF1* (F: TTGACATCATTTTACCGCAGA, R: GGAATCTCTTCTAGTCCACGA), *EIFIα (*F: GGTGTTCAAAGAACATGGGCAAGAG, R: TTTCCCTCTGATGTGACATAACCTC), *TBX3* (F: CTGACCCCGAAATGCCGAAG, R: ACTATAATTCCCCTGCCACGTT), *DPPA2* (F: TACAGAAGGGGTTCGCC, R:

Uncorrected proof

GGTCTGGGATGGGAAAGTG), *GAPDH* (F: AAGTTCCACGGCACAGTCAAG, R: CACCAGCATCACCCCATTT).

2.7 Immunofluorescence staining

Embryos were fixed in 4% paraformaldehyde at room temperature for 30 min, permeabilized with 0.5% Triton X-100 in PBS for 20 min, and blocked with 1% BSA in PBS for 1 h. Samples were then incubated with primary antibodies (1:100, SETDB1, H3K9me3, H3K9ac, TIP60, or p-ATM) overnight at 4°C. After washing in PBS with 0.1% Tween-20, embryos were incubated with Alexa Fluor-conjugated secondary antibodies for 1 h (1:200) at room temperature in the dark. Nuclear DNA was counterstained with DAPI. Images were acquired using a confocal laser scanning microscope (LSM-880, Zeiss, Jena, Germany) processed with Zen software (v3.10; Zeiss, Jena, Germany), and analyzed using ImageJ (NIH, Bethesda, MD, USA).

2.8 Western blot analysis

For each group, about 100–120 embryos were used for protein extraction and lysed in RIPA buffer with protease/phosphatase inhibitors (61012; Thermo Fisher Scientific, Waltham,USA).

uncorrected proof

After 30 min on ice, protein concentration was measured by BCA assay. 8% SDS–PAGE resolved samples (10-20 μg protein), transferred to PVDF membranes, blocked with 5% skim milk, and incubated overnight with primary antibodies (all diluted 1:1,000). HRP-conjugated secondary antibodies (diluted 1:20,000) were applied for 1 h. The membranes were visualized using a charge-coupled device camera and ECL reagents (Bio-Rad, CA, USA), and the bands were quantified using ImageJ as well as analyzed with Nine Alliance Q9 software (version 18.00, Uvitec, Cambridge, UK).

2.9 SETBD1 dsRNA preparation and microinjection

SETDB1 fragments were PCR-amplified from porcine COC cDNA using T7-tagged primers and transcribed in vitro with the MEGAscript T7 Kit (Thermo Fisher Scientific, Waltham, USA). After 10 h transcription and DNase I treatment, dsRNA was purified using Riboclear™ Plus (GeneAll Biotechnology), dissolved in RNase-free water, and stored at –80°C. Approximately 10 pL of 500 ng/μL dsRNA was injected into MII oocytes. GFP dsRNA was used as a control (Kwon et al., 2022). The primer sequences are F: 5’-TAATACGACTCACTATAGGGGGCTGTGACTTCCTCTTCCT-3’, R: 5’-TAATACGACTCACTATAGGGGATACCCCAGCCCTTGTTCT-3’

Uncorrected proof

2.10 TUNEL assay

Embryos were fixed in 3.7% paraformaldehyde for 30 min and washed with PBS containing 0.1% PVA. Permeabilization was done using 0.5% Triton X-100 for 30 min. TUNEL labeling was performed using the In Situ Cell Death Detection Kit, TMR red (Roche) for 2 h in the dark. Nuclei were counterstained with Hoechst 33342 (10 μg/mL), and fluorescence signals were captured as JPEG files using a digital camera (DP72; Olympus, Tokyo, Japan) connected to a fluorescence microscope (IX70; Olympus, Tokyo, Japan), and the images were subsequently analyzed with ImageJ software. The apoptotic index was calculated as the number of TUNEL-positive nuclei divided by the total number of nuclei.

2.11 AlphaFold predictions for protein-protein interactions

To predict protein–protein interactions, full-length protein sequences of SETDB1 (Uniprot ID: A0A4X1SDV8) and HDAC3 (Uniprot ID: A0A287B575) were retrieved from UniProt. For each protein, the top-ranked reviewed Sus scrofa isoform was selected, and its entry identifier was recorded. Structural models were generated using AlphaFold3 (Jumper et al., 2021), and

Uncorrected proof

the three-dimensional interaction interface between SETDB1 and HDAC3 was analyzed and visualized with PyMOL (PyMOL Software, CA, USA).

2.12 Statistical analysis

All experiments were performed with at least three biological replicates, each comprising a minimum of three technical replicates. Representative images of western blot and immunofluorescence are shown in the figures. Data were analyzed using GraphPad Prism 9.0 software (GraphPad Software, San Diego, CA, USA) and are presented as mean ± SEM. Relative values were normalized by setting the control group as 1-fold, and statistical comparisons were performed between the control and treated groups. Statistical significance was determined using Student's t-test, and a p-value < 0.05 was considered statistically significant. SEM values were calculated from at least three independent experiments.

Uncorrected proof

3. Results

3.1 Stage-specific expression of SETDB1 during early porcine embryonic development

To investigate its expression pattern during early embryonic development, SETDB1 mRNA and protein levels were examined. *SETDB1* mRNA expression gradually decreased after the 2C stage (2C: 1.00 vs. 4C: 0.27 ± 0.03 vs. BL: 0.008 ± 0.002; Fig. 1A). Immunofluorescence staining (IF) revealed that SETDB1 is localized in both the cytoplasm and nucleus, with nuclear signals progressively decreasing from the 2-cell (2C) stage through the blastocyst (BL) stage (Fig. 1B), consistent with previous reports (Rapone et al., 2023). Additionally, western blot analysis (WB) demonstrated a significant decrease in total SETDB1 protein levels at the 4-cell (4C) and BL stages (2C: 1.00 vs. 4C: 0.62 ± 0.22 vs. BL: 0.39 ± 0.22; Fig. 1C and D). These results indicate a progressive decrease in SETDB1 expression and nuclear localization after the 2C stage.

3.2 Effect of SETDB1 knockdown on cleavage progression and blastocyst development

To investigate the functional role of SETDB1, SETDB1 dsRNA was microinjected into MII oocytes. Compared to the control group injected with GFP dsRNA, *SETDB1* mRNA levels were significantly reduced in the SETDB1 KD group (Con: 1.00 vs. SETDB1 KD: 0.28 ± 0.07;

uncorrected proof

$P < 0.0001$; Fig. 2B). IF confirmed that SETDB1 protein expression was markedly reduced at the 4C stage following knockdown (Fig. 2C). Consistently, protein levels of SETDB1 were also markedly decreased (Con: 1.00 vs. SETDB1 KD: 0.39 ± 0.23; $P < 0.01$; Fig. 2D and E).

The developmental outcomes of SETDB1-deficient embryos were then assessed. The rate of progression from the 2C to the 4C stage was lower in the SETDB1 KD group than in the control group, and the proportion of embryos reaching the BL stage was also decreased (2C; Con: 87.54 ± 3.04% vs. SETDB1 KD: 82.22 ± 5.87%, 4C; Con: 83.72 ± 4.88% vs. SETDB1 KD: 67.38 ± 9.80%, BL; Con: 41.5 ± 4.71% vs. SETDB1 KD: 19.20 ± 7.21%; Fig. 2F). BL quality was assessed based on total cell number, which was reduced in the SETDB1 KD group compared to the control group (Con: 44.27 ± 8.97 vs. SETDB1 KD: 24.75 ± 10.07; $P < 0.0001$; Fig. 2G and H). Moreover, BL morphology analysis showed that SETDB1 KD embryos formed blastocysts with lower quality compared to controls (Fig. 2I). These findings suggest that SETDB1 is important during the 4C stage, when zygotic genome activation (ZGA) occurs, and contributes to the maintenance of BL quality.

3.3 Effect of SETDB1 knockdown on histone modification and ZGA-related gene expression

Given the marked developmental defects in SETDB1 KD embryos (Fig. 2E-G), we further

uncorrected proof

investigated the underlying molecular mechanisms. Compared to the control group, SETDB1 KD embryos exhibited a clear decrease in H3K9me3 and a concomitant increase in H3K9ac signals (H3K9me3; Con: 1.00 ± 0.00 vs. SETDB1 KD: 0.53 ± 0.06; $P < 0.05$; H3K9ac; Con: 00.99 ± 0.98 vs. SETDB1 KD: 2.10 ± 0.90; $P < 0.01$; Fig. 3A-D). These changes were further confirmed by WB analysis, which revealed reduced H3K9me3 and elevated H3K9ac protein levels in the SETDB1 KD group (H3K9me3; Con: 1.00 vs. SETDB1 KD: 0.50 ± 0.05; $P < 0.05$; H3K9ac; Con: 1.00 vs. SETDB1 KD: 1.31 ± 0.17; $P< 0.01$; Fig. 3E-G).

Additionally, to assess whether SETDB1 KD affects ZGA, the mRNA expression levels of ZGA-related genes were measured at the 4C stage. Quantitative real-time PCR (RT-qPCR) analysis showed that transcript levels of *DPPA2*, *ZSCAN4* and *EIF1α* were all decreased in SETDB1 KD embryos compared to the control (*DPPA2*; Con: 1.00 vs. SETDB1 KD: 0.38 ± 0.12, *ZSCAN4*; Con: 1.00 vs. SETDB1 KD: 0.35 ± 0.09, *EIF1α*; Con: 1.00 vs. SETDB1 KD: 0.47 ± 0.22, *TCSTV3*; Con: 1.00 vs. SETDB1 KD: 0.45 ± 0.10, *RIF1*; Con: 1.00 vs. SETDB1 KD: 0.44 ± 0.06, *TBX3*; Con: 1.00 vs. SETDB1 KD: 0.32 ± 0.13; Fig. 3H). Collectively, these findings suggest that SETDB1 is important for regulating H3K9 modification during early development and that its absence impairs the activation of key ZGA genes at the 4C stage.

3.4 Regulation of SETDB1 in DNA damage repair during early embryonic development

uncorrected proof

To elucidate the role of SETDB1 in DNA repair, embryos were treated with 25 μg/mL etoposide (ETP) to induce DNA damage, followed by recovery in fresh medium. Developmental assessment revealed that both the control and C+ETP groups progressed to the 4C and BL stages, whereas the KD+ETP group exhibited significantly reduced developmental rates at both stages (2C; Con: 85.73 ± 2.98% vs. KD: 82.83 ± 3.20% vs. C+ETP: 81.73 ± 4.00% vs. KD+ETP: 81.8 ± 6.21%, ns; 4C; Con: 73.87 ± 0.98% vs. KD: 64.70 ± 4.98%, $P < 0.05$ vs. C+ETP: 68.37 ± 3.09%, $P < 0.05$ vs. KD+ETP: 54.97 ± 5.34%, $P < 0.05$; BL; Con: 37.10 ± 2.05% vs. KD: 26.27 ± 1.46%, $P < 0.01$ vs. C+ETP: 29.37 ± 2.15%, ns vs. KD+ETP: 23.17 ± 2.01%, $P < 0.01$; Fig. 4A). In addition, TUNEL assay revealed a significant increase in the proportion of TUNEL-positive nuclei in both KD and KD+ETP groups compared with the Con and C+ETP groups. Notably, the KD+ETP group exhibited the highest level of DNA fragmentation and apoptosis, indicating that SETDB1 KD markedly accelerates cell death under DNA damage conditions (Con: 3.22 ± 3.09 vs. C+ETP: 5.84 ± 3.39, $P < 0.001$; Con: 3.22 ± 3.09 vs. KD: 4.11 ± 2.12, $P < 0.05$; Con: 3.22 ± 3.09 vs. KD+ETP: 9.87 ± 4.80, $P < 0.0001$; Fig 4B and C). Consistent with these findings, γH2AX immunofluorescence intensity was significantly increased in the C+ETP group compared with the control, whereas KD+ETP embryos failed to recover and displayed persistently high levels of DNA damage signaling

Uncorrected proof

(γH2AX; Con: 1.00 ± 0.24 vs. C+ETP: 1.80 ± 0.35, $P < 0.001$; Con: 1.00 ± 0.24 vs. KD: 1.09 ± 0.16, ns; Con: 1.00 ± 0.24 vs. KD+ETP: 1.17 ± 0.31, $P < 0.05$; Fig. 4D and E).

Moreover, Quantitative PCR analysis revealed a marked reduction in ZGA-related transcripts in KD and KD+ETP embryos. Specifically, *ZSCAN4* expression was significantly decreased in both KD and KD+ETP groups, with the strongest reduction observed in KD+ETP embryos (*ZSCAN4*; Con: 1.00 ± 0.00 vs. C+ETP: 0.68 ± 0.13, ns vs. KD: 0.58 ± 0.20, $P < 0.05$ vs. KD+ETP: 0.33 ± 0.12, $P < 0.01$). Likewise, *DPPA2* expression was significantly reduced in KD and KD+ETP embryos compared with controls (*DPPA2*; Con: 1.00 ± 0.00 vs. C+ETP: 0.88 ± 0.18, ns vs. KD: 0.49 ± 0.14, $P < 0.05$ vs. KD+ETP: 0.49 ± 0.15, $P < 0.05$; Fig. 4F). These results demonstrate that SETDB1 is important not only for developmental progression but also for maintaining genomic integrity and transcriptional competence during early embryogenesis under DNA damage conditions.

3.5 Role of SETDB1 in DNA damage repair-related protein expression

To further investigate the molecular basis of impaired recovery, the expression and localization of DNA damage repair–related proteins were examined. IF analysis showed that nuclear accumulation and colocalization of TIP60 with H3K9me3 were markedly reduced in

uncorrected proof

KD+ETP embryos compared with C+ETP embryos (Fig. 5A). Moreover, phospho-ATM (p-ATM) levels were significantly decreased in KD+ETP embryos (C+ETP: 0.99 ± 0.22 vs. KD+ETP: 0.57 ± 0.33, $P < 0.001$; Fig. 5B and C).

WB analysis further confirmed that DNA damage response (DDR)-related proteins were upregulated in the C+ETP group compared with control, but markedly reduced in KD and KD+ETP embryos. Specifically, HP1β expression increased after ETP treatment but was significantly decreased in KD and KD+ETP groups (Con: 1.00 vs. KD: 0.45 ± 0.14, $P < 0.01$; Con: 1.00 vs. KD+ETP: 0.51 ± 0.05, $P < 0.01$; Fig. 5D and E). Similarly, TIP60 protein levels were elevated in C+ETP embryos but declined in KD and KD+ETP groups (Con: 1.00 vs. KD: 0.39 ± 0.23, $P < 0.05$; Con: 1.00 vs. KD+ETP: 0.48 ± 0.19, $P < 0.05$; Fig. 5D and F). In line with this, p-ATM expression was also induced in the C+ETP group but significantly suppressed in KD and KD+ETP embryos (Con: 1.00 vs. KD: 0.43 ± 0.22, $P < 0.001$; Con: 1.00 vs. KD+ETP: 0.46 ± 0.10, $P < 0.001$; Fig. 5D and G). Together, these results indicate that SETDB1 KD disrupts DDR signaling by impairing the expression and localization of key repair proteins.

3.6 Impact of HDAC3 inhibition on H3K9me3/H3K9ac levels and SETDB1 protein expression

uncorrected proof

SETDB1 KD reduced H3K9me3 and increased H3K9 acetylation, suggesting that SETDB1-mediated methylation may be linked to histone deacetylation. To test this, HDAC3 was examined for its role in this process. WB analysis revealed a decrease in HDAC3 protein levels following SETDB1 KD compared to the control group (Con: 1 vs. SETDB1 KD: 0.88 ± 0.05; $P < 0.05$; Fig. 6A and B). To determine the appropriate concentration of HDAC3 inhibitor (HDAC3i), a dose–response experiment was conducted. As a result, 0.5 μM was identified as the lowest effective concentration that significantly impaired blastocyst development (Con: 38.4 ± 11.25% vs. 0.5 μM: 25.95 ± 7.79% vs. 1.0 μM: 9.55 ± 5.23%; Fig. 6C). Upon HDAC3i, H3K9ac levels increased while H3K9me3 levels decreased. In addition, SETDB1 protein expression was reduced (H3K9ac; Con: 1 vs. HDAC3i: 1.62 ± 0.06; $P < 0.0001$; H3K9me3; Con: 1 vs. HDAC3i: 0.81 ± 0.10; $P < 0.01$; SETDB1; Con: 1; HDAC3i: 0.68 ± 0.06; $P < 0.001$; Fig. 6D-G), and HDAC3 protein levels were also decreased (Fig. 6H). In addition, AlphaFold analysis predicted plausible indirect interactions between HDAC3 and SETDB1, supporting the possibility of a functional association within a shared regulatory complex (Fig 6I). These findings raise the possibility that HDAC3 activity may contribute to maintaining H3K9 modification and supporting SETDB1 stability.

uncorrected proof

4. Discussion

In this study, we investigated the effects of SETDB1 knockdown (KD) during the zygotic genome activation (ZGA) of porcine embryos by analyzing alterations in histone modification patterns and the expression of DNA damage repair-related proteins.

Repressive histone modifications such as H3K9me3 are typically associated with transcriptional silencing and the heterochromatin formation. The reduction of these marks during the ZGA is recognized as a factor that facilitates transcriptional activation (Matoba et al., 2014; Sankar et al., 2020). However, the results showed that SETDB1 KD led to a significant decrease in H3K9me3 levels and, unexpectedly, a concurrent downregulation of ZGA-related gene expression (Fig. 3H). This suggests that the reduction of ZGA-related transcripts reflects an insufficient chromatin environment for proper transcriptional activation, in which H3K9me3 plays a critical role (Yu et al., 2022). Consistent with this notion, a progressive decrease in SETDB1 expression was observed, accompanied by reduced H3K9me3 levels during embryonic development. Such a decline has been reported to promote global chromatin remodeling required for transcriptional activation up to the blastocyst stage (Li et al., 2023; Xu et al., 2023). These findings further support this model by reinforcing the functional link between SETDB1-mediated H3K9me3 regulation and chromatin dynamics

uncorrected proof

during ZGA. Given that ZGA represents a developmental stage highly vulnerable to DNA damage, these findings indicate that H3K9me3 is required not only for transcriptional competence but also for sustaining an adequate DNA damage response (DDR) during early embryogenesis.

Similar to SUV39H1-dependent DDR signaling, in which H3K9me3 facilitates HP1β recruitment to DNA damage sites (Ayrapetov et al., 2014), SETDB1 may also contribute to chromatin-based repair by performing a comparable function. In the present study, embryos subjected to SETDB1 KD combined with etoposide (ETP) treatment showed a marked decrease in HP1β expression (Fig. 5D and E), implying impaired heterochromatin stability and defective repair of DNA double strand breaks (DSBs). ETP treatment at the zygotic stage has been employed in previous studies, which demonstrated that DNA damage induced at this early stage can be propagated through cleavage divisions and ultimately affect later developmental outcomes (Wang et al., 2015). Importantly, ETP acts as a topoisomerase II inhibitor that stabilizes the cleavage complex and prevents re-ligation, thereby converting transient DNA breaks into persistent DSBs (Canela et al., 2019). HP1β binds specifically to H3K9me3 and serves as a chromatin platform for the recruitment of repair factors (Maeda and Tachibana, 2022). Moreover, SETDB1 has been shown to suppress transcription at DSBs sites during

uncorrected proof

meiosis in mouse X chromosomes via H3K9me3 deposition and HP1β recruitment (Hirota et al., 2018), and to maintain higher-order chromatin integrity in UV-damaged heterochromatin. These studies support the broader role of SETDB1 in chromatin-based DDR.

The H3K9me3–mediated repair pathway plays an essential role in initiating DDR (Tu et al., 2020). In this study, SETDB1 KD disrupted this pathway (Fig. 5A-G). γH2AX is a central marker of DNA damage, accumulating at DSBs sites proportionally to damage severity and facilitating recruitment of DNA damage repair proteins (Mah et al., 2010; Rogakou et al., 1998). Unexpectedly, γH2AX levels were reduced rather than increased in SETDB1 KD embryos, suggesting a failure to activate DDR signaling, potentially due to impaired ATM activation or reduced TIP60 activity (Murr et al., 2006).

The ZGA stage is characterized by a marked elevation in transcriptional activity, which increases the risk of DSBs formation due to R-loop formation and transcription-replication conflicts (Aguilera and García-Muse, 2012; Butuči et al., 2015). During this period, embryos must independently maintain genome integrity, and any disruption of the repair system may interfere with transcriptional reprogramming and compromise developmental competence (Chen et al., 2023). Taken together, these findings indicate that SETDB1 plays an essential role in maintaining a functional DDR during ZGA, likely through its role in facilitating chromatin-

uncorrected proof

based repair processes. Taken together, these findings indicate that SETDB1 plays an essential role in maintaining a functional DDR during ZGA, likely through facilitation of chromatin-based repair processes. In addition, SETDB1 may stabilize heterochromatin structure via H3K9me3 and promote HP1β recruitment, thereby preventing uncontrolled transcription and safeguarding genome integrity. Such stabilization is particularly critical during ZGA, when widespread transcriptional activation heightens the risk of DNA damage and requires a balanced chromatin environment for successful reprogramming (Kim et al., 2016).

The findings further suggest that HDAC3, which regulates histone modifications, may functionally interact with SETDB1 during ZGA (Fig. 6I). HDAC3 activity may contribute to maintaining the balance of H3K9 acetylation and methylation and to stabilizing SETDB1 protein levels. Previous chromatin profiling studies reported co-localization of SETDB1, HDAC3, and KAP1 at genomic regions enriched for H3K9me3 and H3K14ac, implying functional cooperation. These observations are consistent with a model in which SETDB1 and HDAC3 contribute to stable chromatin remodeling in early embryos. Future studies should examine whether additional histone deacetylases (HDACs) or histone acetyltransferases (HATs) participate in this regulatory network, and whether this mechanism is conserved across species.

uncorrected proof

In conclusion, these results demonstrate that SETDB1 is essential for maintaining an H3K9me3-dependent heterochromatin environment that supports proper histone modifications and DNA damage repair during the ZGA of porcine embryos. These findings extend the conservation of this mechanism by showing that SETDB1 KD impairs DDR signaling and heterochromatin stability in porcine embryos, a species in which such research has been relatively underexplored. Furthermore, our data raise the possibility that HDAC3 may cooperate with SETDB1 to regulate the acetylation–methylation balance of H3K9, providing preliminary mechanistic insight into epigenetic regulation during early development and underscoring the need for further biochemical and chromatin-based studies. Collectively, this study supports the notion that SETDB1-mediated chromatin remodeling may represent a conserved mechanism that helps safeguard genome stability during embryogenesis (Bhaskara et al., 2010).

Funding

This research was supported by the National Research Foundation (NRF) of Korea grant funded by the Korean government (MSIT) (2022R1A2C300769) and the Korea Research Institute of Bioscience and Biotechnology (KRIBB) Research Initiative Program (KGM5162524).

uncorrected proof

Authors contributions

Hyeon-Ji Song conceptualized the study, developed the methodology, and wrote the original draft. Xiang-Shun Cui supervised the research, reviewed and edited the manuscript, and contributed to the formal analysis. Song-Hee Lee and Lu Qin-Yue assisted with data analysis. Cheng-Lin Zhan and Gyu-Hyun Lee managed the software and data curation. Jae-Min Sim provided resources. Ji-Su Kim and Yu-Jin Jo assisted in the revision of the manuscript. All authors reviewed and approved the final manuscript.

Conflict of interest statement

The Authors have no conflicts of interest to declare.

Instructions on the experimental animal

The ovaries were sourced from sows at a local slaughterhouse, and oocytes were used for the experiment. Thus, this study did not involve live animal experimentation

uncorrected proof

Figure legends

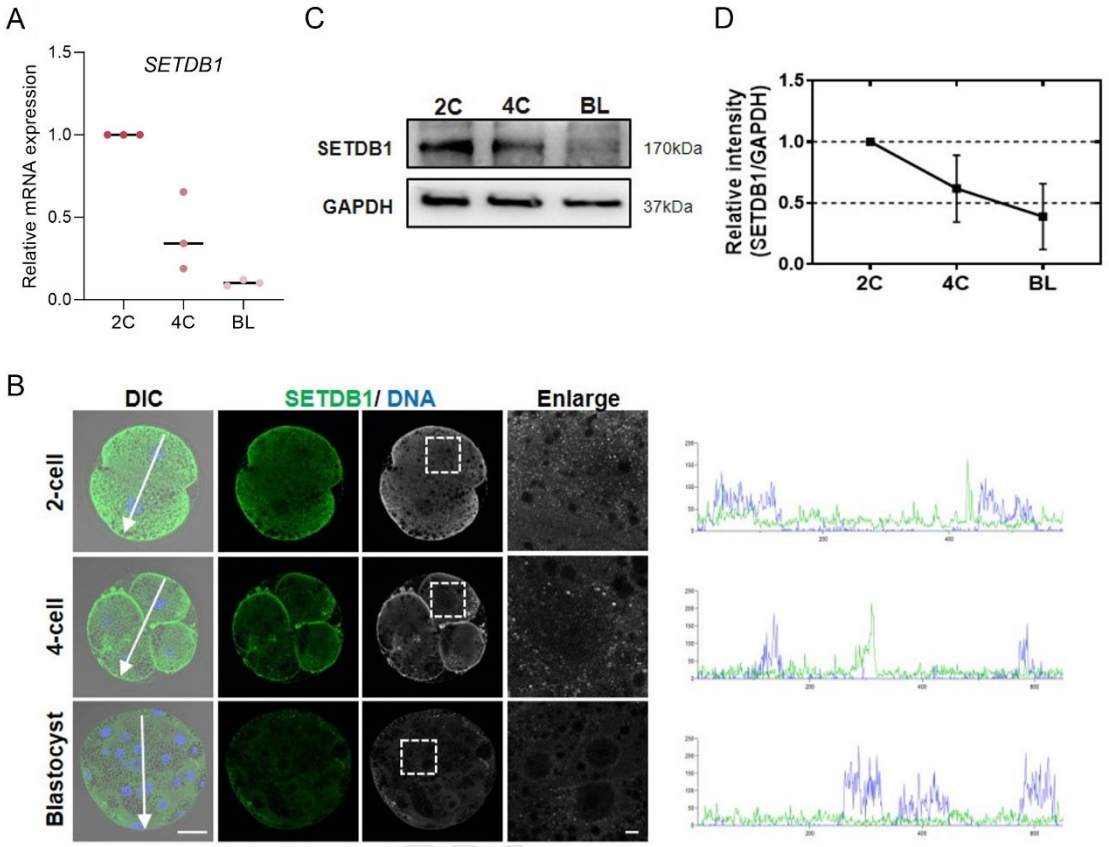

Figure 1. SETDB1 expression altered after the 2C stage in porcine embryos

A: Relative expression of *SETDB1* mRNA in 2-cell (2C), 4-cell (4C), and Blastocyst (BL) stage embryos. B: Representative immunofluorescence staining (IF) images of SETDB1 protein from the 2C to BL stages, along with fluorescence intensity profiles of SETDB1 and DNA measured along the white line. C: Western blot (WB) images of SETDB1 protein from the 2C to BL stages. GAPDH was used as the internal reference protein. D: Relative protein levels of SETDB1. Scale bar: 20 μm.

uncorrected

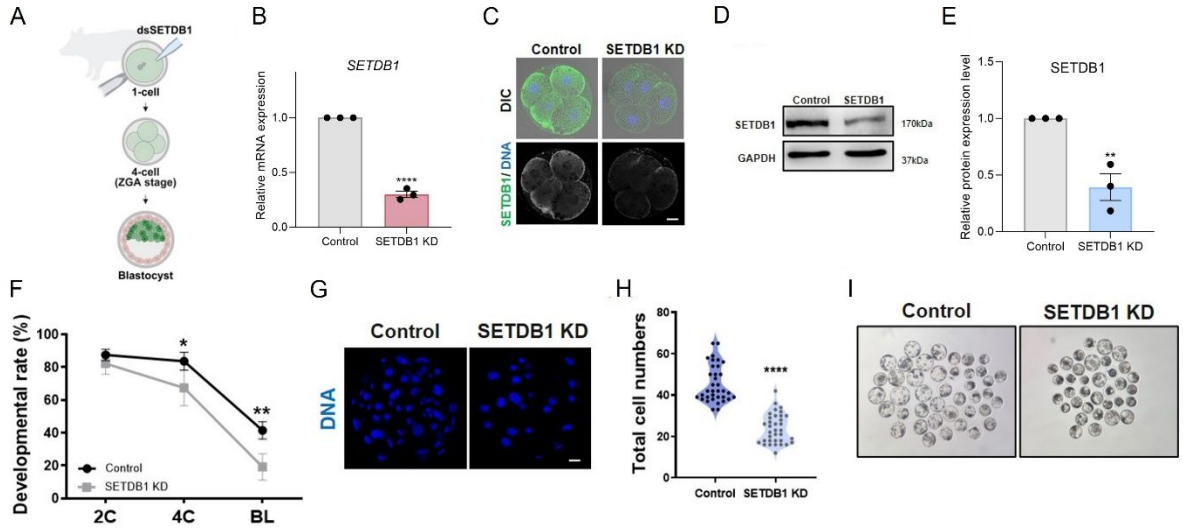

Figure 2. SETDB1 KD impaired embryonic cleavage and blastocyst formation

A: Schematic representation of SETDB1 knockdown (KD) by dsRNA microinjection and developmental progression. B: Relative mRNA expression levels of *SETDB1* at the 4C stage in the control group (GFP dsRNA) and SETDB1 KD group ($P < 0.0001$). C: Representative IF images showing reduced SETDB1 protein expression in SETDB1 KD embryos at the 4C stage. D: Representative Western blot images showing SETDB1 and GAPDH protein levels. E: Quantification of SETDB1 protein expression normalized to GAPDH ($P < 0.01$). F: Developmental progression from the 2C, 4C and BL stages. G: Quantification of total cell numbers in BL from control (n=32) and SETDB1 KD (n=32) groups. H: Violin plot showing the distribution of total cell numbers per BL ($p < 0.0001$). I: Representative brightfield images of BL morphology in control and SETDB1 KD groups, showing reduced blastocyst quality after SETDB1 KD. Scale bar: 20 μm. *: $P < 0.05$; **: $P < 0.01$; ****: $P < 0.0001$.

Uncorrected Proof

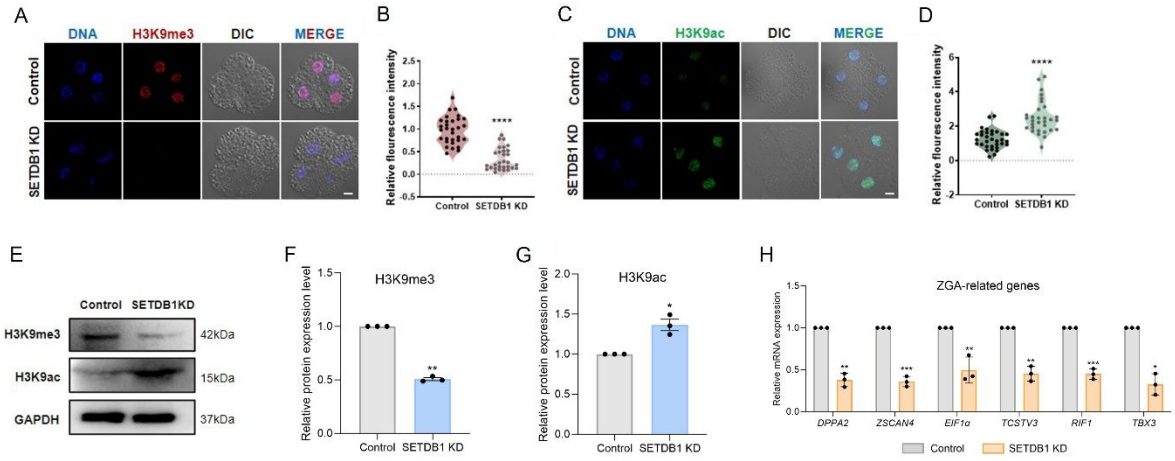

Figure 3. SETDB1 was required for H3K9me3 maintenance and ZGA gene at the 4C stage

A: IF staining images of H3K9me3 and DNA at the 4C stage with brightfield images. B: Quantification of H3K9me3 fluorescence intensity in control (n=31) and SETDB1 KD (n=30) embryos ($P < 0.05$). C: Representative IF images of H3K9ac and DNA. D: Quantification of H3K9ac fluorescence intensity in control (n=33) and SETDB1 KD (n=31) embryos ($P < 0.01$). E: Representative WB images of H3K9me3, H3K9ac, and GAPDH. F: Quantification of H3K9me3 protein levels normalized to GAPDH ($P < 0.05$). G: Quantification of H3K9ac protein levels normalized to GAPDH ($P < 0.01$). H: Relative mRNA expression levels of *DPPA2* ($P < 0.01$), *ZSCAN4* ($P < 0.001$) and *EIF1α* ($P < 0.01$), *TCSTV3* ($P < 0.01$), *RIF1* ($P < 0.001$), *TBX3* ($P < 0.05$) measured by RT-qPCR. I: SETDB1 KD reduces H3K9me3 and increases H3K9ac, leading to impaired expression of ZGA-related genes. However, the exact mechanism linking H3K9me3 loss to ZGA failure, and the reason for H3K9ac accumulation, remain unclear. Scale bar: 20 μm. *: $P < 0.05$; **: $P < 0.01$; ***: $P < 0.001$; ****: $P < 0.0001$.

Uncorrected Proof

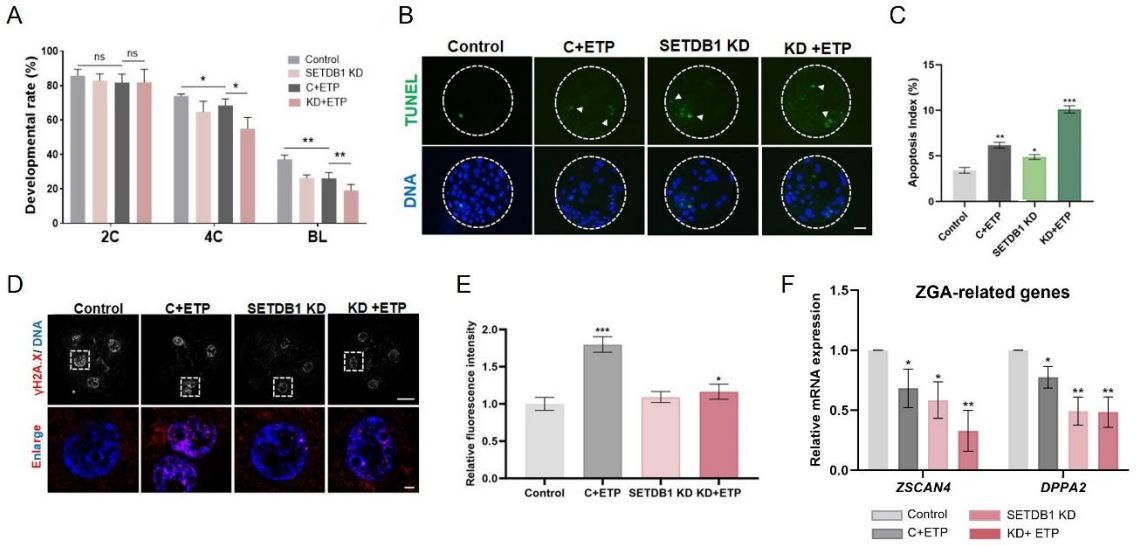

Figure 4. SETDB1 KD reduced embryo recovery following etoposide-induced DNA damage

A: Developmental rates at the 2C, 4C and BL stages following etoposide treatment (2C; Con vs. KD vs. C+ETP, ns vs. KD+ETP, ns; 4C; Con: vs. KD, $P < 0.05$ vs. C+ETP, $P < 0.05$ vs. KD+ETP, $P < 0.05$; BL; Con vs. KD, $P < 0.01$ vs. C+ETP, ns vs. KD+ETP, $P < 0.01$). B: Representative TUNEL staining images showing apoptotic nuclei. White arrows indicate TUNEL-positive cells. C: Quantification of the percentage of TUNEL-positive nuclei across Con, C+ETP, KD, and KD+ETP embryos (Control; n=30, C+ETP; n=30, KD; n=30, KD+ETP; n=31). D: Representative immunofluorescence images of γH2AX and DNA. E: Quantification of γH2AX fluorescence intensity normalized to control (Con vs. C+ETP, $P < 0.001$; Con vs. KD, $P < 0.05$; Con vs. KD+ETP, $P < 0.0001$; Control; n=30, C+ETP; n=31, KD; n=30, KD+ETP; n=30). F: Relative mRNA expression levels of *ZSCAN4* and *DPPA2* in Con, C+ETP, KD, and KD+ETP embryos (*ZSCAN4*; Con vs. C+ETP, ns vs. KD, $P < 0.05$ vs. KD+ETP, $P < 0.01$; *DPPA2*; Con vs. C+ETP, ns vs. KD, $P < 0.05$ vs. KD+ETP, $P < 0.05$). Scale bar: 20 μm. ns: Not significant; *: $P < 0.05$; **: $P < 0.01$; ***: $P < 0.001$; ****: $P < 0.0001$.

Uncorrected proof

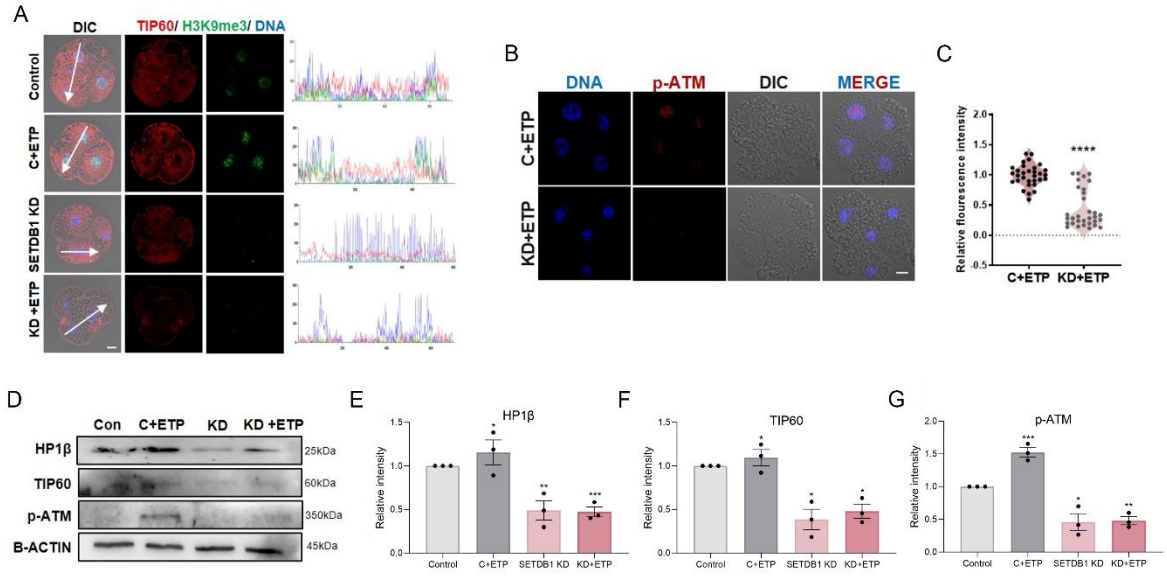

Figure 5. SETDB1 KD impaired DNA damage response by downregulating DNA damage repair-related proteins

A: Representative IF images of all four groups (Con, C+ETP, KD, and KD+ETP), showing nuclear accumulation and colocalization of TIP60 with H3K9me3 and DNA. Line-scan profiles indicate fluorescence intensity along the white dashed line. B: Representative IF images of p-ATM and DNA in C+ETP and KD+ETP embryos, with corresponding DIC and merged images. C: Quantification of p-ATM fluorescence intensity in C+ETP (n=31) and KD+ETP (n=32) embryos ($P < 0.001$). D: Representative WB images of HP1β, TIP60, and p-ATM protein expression. GAPDH was used as a loading control. E–G: Quantification of protein levels for HP1β (E; Con vs. KD, $P < 0.01$; Con vs. KD+ETP, $P < 0.01$), TIP60 (F; Con s. KD, $P < 0.05$; Con vs. KD+ETP, $P < 0.05$) and p-ATM (G; Con s. KD, $P < 0.001$; Con vs. KD+ETP, $P < 0.001$) normalized to GAPDH. Scale bar: 20 μm. ns: Not significant; *: $P < 0.05$; **: $P < 0.01$; ***: $P < 0.001$; ****: $P < 0.0001$.

Uncorrected Proof

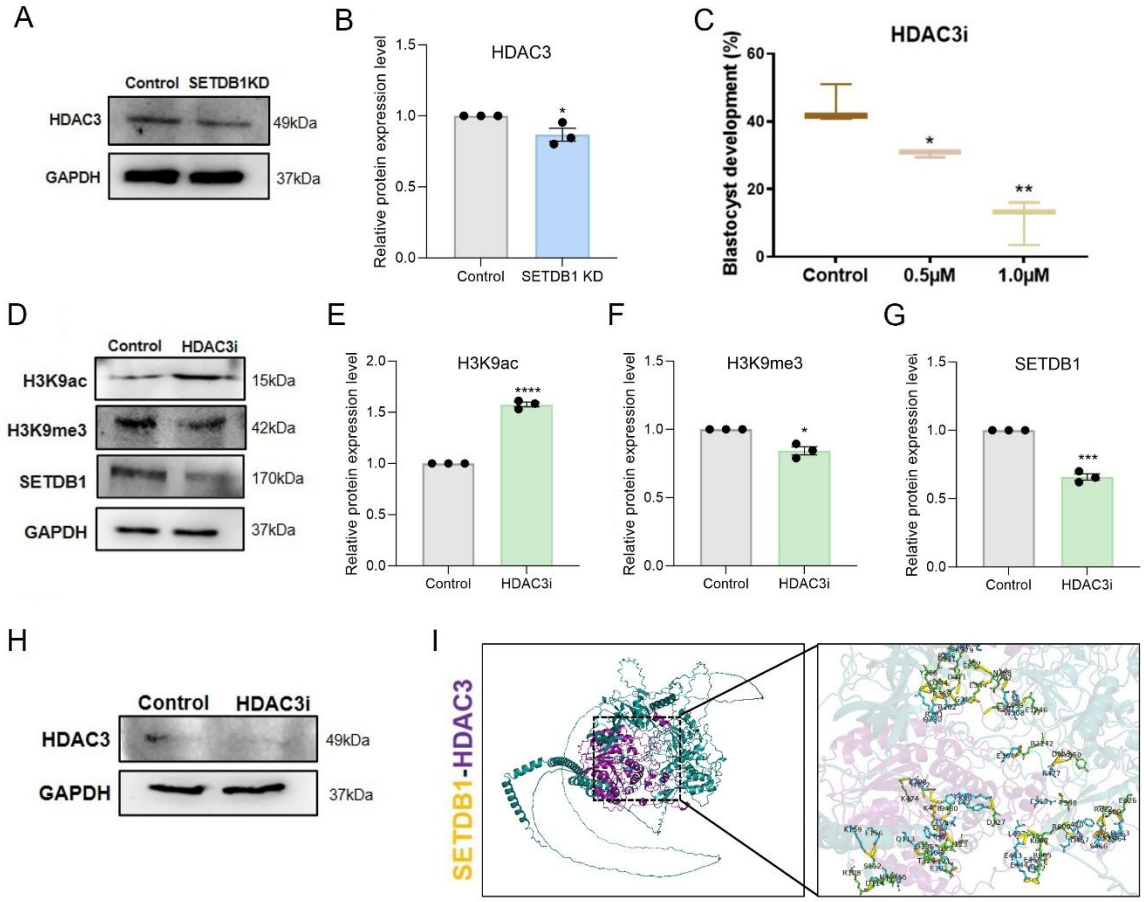

Figure 6. HDAC3 activity influenced H3K9 modification and stabilized SETDB1 expression

A: Representative WB images of HDAC3 and GAPDH. B: Quantification of HDAC3 protein levels normalized to GAPDH ($P < 0.05$). C: Dose-dependent effect of HDAC3 inhibitor on BL rate (Con vs. 0.5 μM, $P < 0.05$ vs. 1.0 μM, $P < 0.01$). D: Representative western blot images of H3K9ac, H3K9me3, SETDB1. E: Quantification of H3K9ac levels ($P < 0.0001$). F: Quantification of H3K9me3 levels normalized to GAPDH. G: Quantification of SETDB1 protein levels normalized to GAPDH ($P < 0.001$). H: Quantification of HDAC3 protein levels following HDAC3 inhibition. I: AlphaFold-based prediction of an indirect interaction between HDAC3 and SETDB1. ns: Not significant; *: $P < 0.05$; **: $P < 0.01$; ***: $P < 0.001$; ****: $P < 0.0001$.

Uncorrected

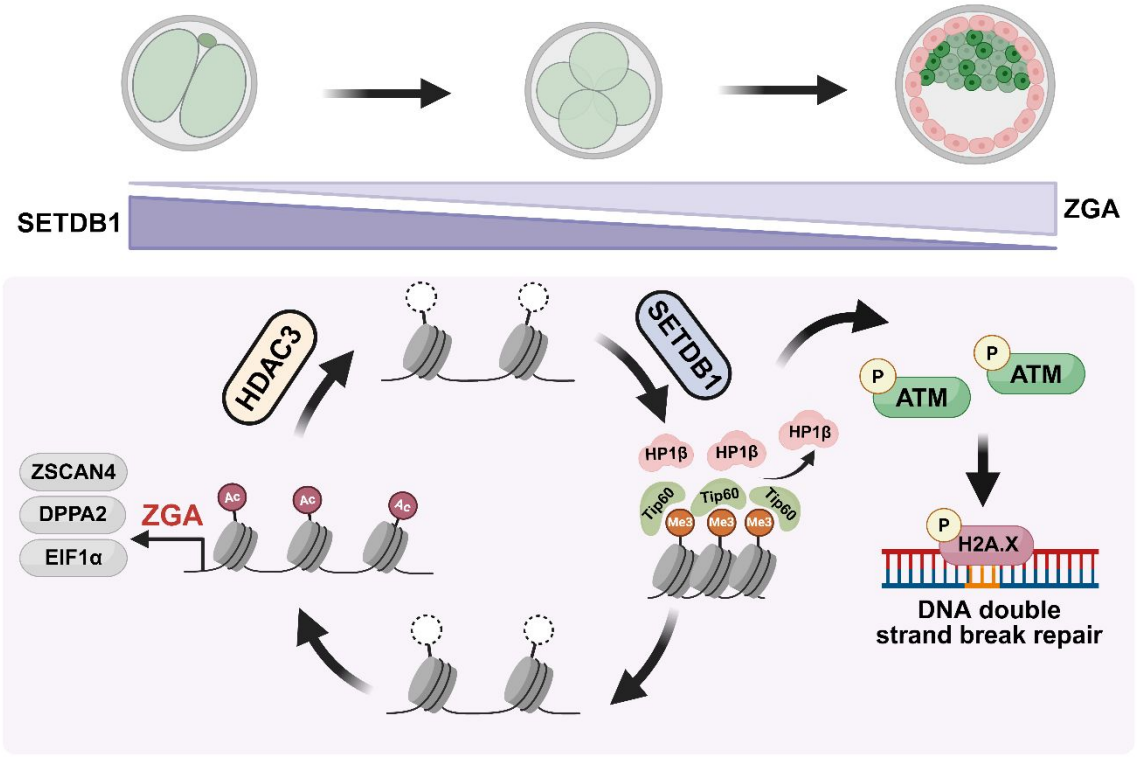

Figure 7. Schematic diagram illustrating the cooperative role of SETDB1 and HDAC3 in regulating histone modifications and genome stability during porcine preimplantation development

During embryonic development, SETDB1 and HDAC3 together maintain the histone H3K9 modifications. HDAC3 removes H3K9ac, preserving a deacetylated state. SETDB1 deposits H3K9me3, promoting heterochromatin formation and transcriptional repression. SETDB1-mediated H3K9me3 also recruits HP1β and Tip60, which facilitate ATM activation and γH2AX phosphorylation at DNA double-strand break sites. Disruption of this axis impairs ZGA gene expression and the DNA damage response. Figure created with BioRender.com.

Uncorrected

References

Aguilera A & García-Muse T. 2012. R loops: from transcription byproducts to threats to genome stability. *Molecular Cell*, **46**(2): 115-124. DOI: 10.1016/j.molcel.2012.04.009

Ayrapetov MK, Gursoy-Yuzugullu O, Xu C, et al. 2014. DNA double-strand breaks promote methylation of histone H3 on lysine 9 and transient formation of repressive chromatin. *Proceedings of the National Academy of Science of the United States of America*, **111**(25): 9169-9174. DOI: 10.1073/pnas.1403565111

Bhaskara S, Knutson SK, Jiang G, et al. 2010. Hdac3 Is Essential for the Maintenance of Chromatin Structure and Genome Stability. *Cancer Cell*, **18**(5): 436-447. DOI: https://doi.org/10.1016/j.ccr.2010.10.022

Bure IV, Nemtsova MV, Kuznetsova EB. 2022. Histone Modifications and Non-Coding RNAs: Mutual Epigenetic Regulation and Role in Pathogenesis. *International Journal of Molecular Sciences*, **23**(10). DOI: 10.3390/ijms23105801

Butuči M, Williams AB, Wong MM, et al. 2015. Zygotic Genome Activation Triggers Chromosome Damage and Checkpoint Signaling in C. elegans Primordial Germ Cells. *Developmental Cell*, **34**(1): 85-95. DOI: 10.1016/j.devcel.2015.04.019

Canela A, Maman Y, Huang SN, et al. 2019. Topoisomerase II-Induced Chromosome Breakage and Translocation Is Determined by Chromosome Architecture and Transcriptional Activity. *Molecular Cell*, **75**(2): 252-266.e258. DOI: 10.1016/j.molcel.2019.04.030

Chen Y, Wang L, Guo F, et al. 2023. Epigenetic reprogramming during the maternal-to-zygotic transition. *MedComm (2020)*, **4**(4): e331. DOI: 10.1002/mco2.331

Cockburn K & Rossant J. 2010. Making the blastocyst: lessons from the mouse. *Journal of*

Uncorrected proof

Clinical Investigation, **120**(4): 995-1003. DOI: 10.1172/jci41229

Gelato KA & Fischle W. 2008. Role of histone modifications in defining chromatin structure and function. *Biological Chemistry*, **389**(4): 353-363. DOI: 10.1515/BC.2008.048

Gibney ER & Nolan CM. 2010. Epigenetics and gene expression. *Heredity (Edinb)*, **105**(1): 4-13. DOI: 10.1038/hdy.2010.54

Hirota T, Blakeley P, Sangrithi MN, et al. 2018. SETDB1 Links the Meiotic DNA Damage Response to Sex Chromosome Silencing in Mice. *Developmental Cell*, **47**(5): 645-659.e646. DOI: 10.1016/j.devcel.2018.10.004

Jumper J, Evans R, Pritzel A, et al. 2021. Highly accurate protein structure prediction with AlphaFold. *Nature*, **596**(7873): 583-589. DOI: 10.1038/s41586-021-03819-2

Kim J, Zhao H, Dan J, et al. 2016. Maternal Setdb1 Is Required for Meiotic Progression and Preimplantation Development in Mouse. *PLoS Genetics*, **12**(4): e1005970. DOI: 10.1371/journal.pgen.1005970

Kim MJ, Jeon SB, Kang HG, et al. 2024. Cadmium exposure impairs porcine embryonic development by inducing oxidative stress and mitochondrial dysfunction. *Journal of Animal Reproduction and Biotechnology*, **39**(1): 48-57. DOI: 10.12750/JARB.39.1.48

Kwon J, Jo Y-J, Yoon S-B, et al. 2022. M⁶A reader hnRNPA2/B1 is essential for porcine embryo development via gene expression regulation. *Journal of Animal Reproduction and Biotechnology*, **37**(2): 121-129. DOI: 10.12750/JARB.37.2.121

Li H, Sun J, Dong Y, et al. 2023. Remodeling of H3K9me3 during the pluripotent to totipotent-like state transition. *Stem Cell Reports*, **18**(2): 449-462. DOI: 10.1016/j.stemcr.2022.12.006

Liu B, Wang Z, Zhang L, et al. 2013. Depleting the methyltransferase Suv39h1 improves DNA

Uncorrected proof

repair and extends lifespan in a progeria mouse model. *Nature Communication*, **4**: 1868. DOI: 10.1038/ncomms2885

Ma G, Gao A, Chen J, et al. 2024. Modeling high-risk Wilms tumors enables the discovery of therapeutic vulnerability. *Cell Reports Medicine*, **5**(10): 101770. DOI: 10.1016/j.xcrm.2024.101770

Maeda R & Tachibana M. 2022. HP1 maintains protein stability of H3K9 methyltransferases and demethylases. *EMBO Reports*, **23**(4): e53581. DOI: 10.15252/embr.202153581

Mah LJ, El-Osta A, Karagiannis TC. 2010. gammaH2AX: a sensitive molecular marker of DNA damage and repair. *Leukemia*, **24**(4): 679-686. DOI: 10.1038/leu.2010.6

Matoba S, Liu Y, Lu F, et al. 2014. Embryonic development following somatic cell nuclear transfer impeded by persisting histone methylation. *Cell*, **159**(4): 884-895. DOI: 10.1016/j.cell.2014.09.055

Murr R, Loizou JI, Yang YG, et al. 2006. Histone acetylation by Trrap-Tip60 modulates loading of repair proteins and repair of DNA double-strand breaks. *Nature Cell Biology*, **8**(1): 91-99. DOI: 10.1038/ncb1343

Musson R, Gąsior Ł, Bisogno S, et al. 2022. DNA damage in preimplantation embryos and gametes: specification, clinical relevance and repair strategies. *Human Reproduction Update*, **28**(3): 376-399. DOI: 10.1093/humupd/dmab046

Prashanth S, Radha Maniswami R, Rajajeyabalachandran G, et al. 2024. SETDB1, an H3K9-specific methyltransferase: An attractive epigenetic target to combat cancer. *Drug Discovery Today*, **29**(5): 103982. DOI: https://doi.org/10.1016/j.drudis.2024.103982

Price AJ, Manjegowda MC, Kain J, et al. 2020. Hdac3, Setdb1, and Kap1 mark

Uncorrected proof

H3K9me3/H3K14ac bivalent regions in young and aged liver. *Aging Cell*, **19**(2): e13092. DOI: 10.1111/acel.13092

Rapone R, Del Maestro L, Bouyioukos C, et al. 2023. The cytoplasmic fraction of the histone lysine methyltransferase Setdb1 is essential for embryonic stem cells. *iScience*, **26**(8): 107386. DOI: 10.1016/j.isci.2023.107386

Rogakou EP, Pilch DR, Orr AH, et al. 1998. DNA double-stranded breaks induce histone H2AX phosphorylation on serine 139. *Journal of Biological Chemistry*, **273**(10): 5858-5868. DOI: 10.1074/jbc.273.10.5858

Sankar A, Lerdrup M, Manaf A, et al. 2020. KDM4A regulates the maternal-to-zygotic transition by protecting broad H3K4me3 domains from H3K9me3 invasion in oocytes. *Nature Cell Biology*, **22**(4): 380-388. DOI: 10.1038/s41556-020-0494-z

Schulz KN & Harrison MM. 2019. Mechanisms regulating zygotic genome activation. *Nature Reviews Genetics*, **20**(4): 221-234. DOI: 10.1038/s41576-018-0087-x

Song HJ. 2025. Functional Insights into SETDB1 during Early Porcine Embryonic Development. Master's Thesis, Chungbuk National University. Cheongju-si, South Korea.

Sinha KK, Bilokapic S, Du Y, et al. 2023. Histone modifications regulate pioneer transcription factor cooperativity. *Nature*, **619**(7969): 378-384. DOI: 10.1038/s41586-023-06112-6

Tu B, Bao Y, Tang M, et al. 2020. TIP60 recruits SUV39H1 to chromatin to maintain heterochromatin genome stability and resist hydrogen peroxide-induced cytotoxicity. *Genome Instability & Disease*, **1**(6): 339-355. DOI: 10.1007/s42764-020-00025-8

Wang H, Luo Y, Lin Z, et al. 2015. Effect of ATM and HDAC Inhibition on Etoposide-Induced

uncorrected proof

DNA Damage in Porcine Early Preimplantation Embryos. *PLoS One*, **10**(11): e0142561. DOI: 10.1371/journal.pone.0142561

Wang X, Fang Y, Liang W, et al. 2024. Fusobacterium nucleatum facilitates anti-PD-1 therapy in microsatellite stable colorectal cancer. *Cancer Cell*, **42**(10): 1729-1746.e1728. DOI: 10.1016/j.ccell.2024.08.019

Wyatt CDR, Pernaute B, Gohr A, et al. 2022. A developmentally programmed splicing failure contributes to DNA damage response attenuation during mammalian zygotic genome activation. *Science Advance*, **8**(15): eabn4935. DOI: 10.1126/sciadv.abn4935

Xu R, Zhu Q, Zhao Y, et al. 2023. Unreprogrammed H3K9me3 prevents minor zygotic genome activation and lineage commitment in SCNT embryos. *Nature Communication*, **14**(1): 4807. DOI: 10.1038/s41467-023-40496-3

Yu H, Chen M, Hu Y, et al. 2022. Dynamic reprogramming of H3K9me3 at hominoid-specific retrotransposons during human preimplantation development. *Cell Stem Cell*, **29**(7): 1031-1050.e1012. DOI: 10.1016/j.stem.2022.06.006

Zhang T, Cooper S, Brockdorff N. 2015. The interplay of histone modifications - writers that read. *EMBO Reports*, **16**(11): 1467-1481. DOI: 10.15252/embr.201540945

uncorrected proof